Fitness seascapes facilitate the prediction of therapy resistance under time-varying selection

Eshan S. King[1], Julia Pelesko[2], Jeff Maltas[2], Steph J. Owen[2], Emily Dolson[3], and Jacob G. Scott[2,*]

[1]Systems Biology and Bioinformatics Program, School of Medicine, Case Western Reserve University, Cleveland, OH, USA
[2]Department of Translational Hematology and Oncology Research, Cleveland Clinic, Cleveland, OH, USA
[3]Department of Computer Science and Engineering, Michigan State University College of Engineering, Lansing, MI, USA
[*]scottj10@ccf.org

ABSTRACT

Predicting the evolution of drug resistance in infectious diseases may enable us to make rational drug choices to avoid resistance and exploit known molecular mechanisms of resistance. Fitness landscapes are commonly used in computational studies to model the genotype-fitness mapping. Canonical fitness landscapes do not intrinsically model varying selection pressure. However, a challenge to predicting the emergence of drug resistance is that disease agents in a patient will never experience a constant environment – the selection pressure imposed by a drug will vary as a result of the drug pharmacokinetic profile, dosing schedule, and spatial concentration gradient. Furthermore, because of evolutionary costs of resistance and different levels of genotype-specific resistance, different drug concentrations may be optimal for the fitness of different genotypes. Explicit modeling of these trade-offs and the resulting rank-order changes in fitness may be important to accurately predict the evolution of a disease population within a patient or other heterogeneous environments. Fitness seascapes extend the fitness landscape model by allowing the mapping to vary according to an arbitrary environmental parameter (e.g., drug concentration), allowing us to model the evolution of resistance with realistic pharmacological considerations. Here, we explore the importance and utility of fitness seascapes in predicting the emergence of resistance. First, we show how modeling genotype-specific dose response curves is necessary to accurately predict evolutionary outcomes in changing environments. Then, using an empirical fitness seascape measured in engineered *E. coli*, we performed computational experiments observing the impact of the rate of change in drug concentration and simulated patient nonadherence on the probability of evolutionary escape. We found that a greater rate of change in drug concentration resulted in a lower rate of resistance, or a lower rate of evolutionary escape. In simulated patients, higher rates of drug regimen nonadherence were associated with greater rates of resistance. Our work integrates an empirical fitness seascape into an evolutionary model with realistic pharmacological considerations. Future work may leverage this platform to optimize dosing regimens or design adaptive therapies to avoid resistance.

Introduction

The evolution of treatment resistance in disease agents across kingdoms, including in cancer and infectious disease, is governed by the same fundamental evolutionary laws. Strategies that leverage evolutionary knowledge may expand our available tools to fight these diseases. Evolutionary medicine is a field that studies how disease agents evolve resistance within and among human hosts. Researchers within evolutionary medicine leverage knowledge of evolutionary processes to develop new treatments and improve existing paradigms[1–3]. Recently, computational studies of the evolution of resistance have been used to optimise dosing schedules *in silico*, *in vitro*, and in clinical trials[4–8].

Fitness landscapes are mappings from genotype to fitness, often used to understand, simulate, and predict evolution[9–14]. Fitness landscapes extend additive models of fitness by allowing genetic epistasis, where the presence of one mutation modulates the effect of another. An assumption of the fitness landscape model is that, for a given landscape, the environment is static[11]. As such, canonical fitness landscapes cannot model evolution under continuously varying selection pressure, such as the rising and falling concentration of drug in a patient over time. This limitation precludes the modeling of evolutionary trade-offs, or fitness costs, where a mutant "trades" a lower fitness in the absence of a drug in exchange for resistance at higher concentrations of the drug[15–17]. Such tradeoffs across environments are common in evolutionary medicine; drug resistance mechanisms often impose metabolic burdens or impair vital functions of the organism – when the drug-selective pressure is removed, the sensitive genotype may have a higher relative fitness and the resistant genotype may go extinct[18,19]. Moreover, disease agents in a patient will never experience a constant environment – the drug concentration will vary according to the pharmacokinetic

profile, dosing schedule, and spatial distribution. Fitness landscapes cannot be naturally applied to these temporally- and spatially-varying dynamics. To address this problem, fitness seascapes extend the fitness landscape model by considering a mapping from both genotype and environment (i.e. drug concentration) to fitness[20–25]. In this work, we model fitness seascapes as collections of genotype-specific dose-response curves. This approach permits the modeling of fitness trade-offs across a range of drug concentrations, allowing us to model the evolution of resistance with realistic pharmacological considerations.

Here, we explore the function and utility of fitness seascapes with empirical growth rate data and computational experiments. First, using simulated fitness seascapes, we demonstrate the necessity of modeling fitness trade-offs in a changing environment by comparing a realistic seascape with trade-offs to a "null" seascape, where we enforce a "no trade-off" condition– what one may implicitly assume when modeling evolution under varying selection with canonical fitness landscapes. Then, we measure an empirical fitness seascape in genetically engineered *E. coli* (Fig. 2), finding evidence for evolutionary trade-offs, or fitness costs to resistance. Using this empirical fitness seascape, we model the emergence of resistance in two drug dosing experiments. In the first experiment, we analyze the impact of the rate of change in drug concentration on the probability of survival and resistance. In the second, we analyze the impact of drug regimen non-adherence in simulated patients on resistance and survival of the infectious agent. Rosenbloom et al[26] have previously explored the relationship between drug regimen adherence and resistance in a computational model of HIV using a two-genotype model. However, there is a lack of computational models that can be applied to other diseases that can help us to explore the relationship between drug regimens and therapy resistance. Our study extends their experimental design into the fitness seascape model with an arbitrary number of genotypes, expanding the flexibility and tractability of this type of study without significantly increasing the complexity. Our work demonstrates that dose-response data is important for accurately modeling the emergence of resistance under varying selective pressure, which is a significant consideration for designing adaptive therapies in the context of evolutionary medicine.

Results

Fitness tradeoffs shape evolutionary response to treatment

We first explored the importance of evolutionary trade-offs, which are naturally modeled by fitness seascapes, in predicting the emergence of therapy resistance. In contrast, canonical fitness landscapes cannot intrinsically model these trade-offs. To investigate these trade-offs, we simulated a random "null seascape", which has a genotype rank-preserving constraint, and a natural seascape, which has no such constraint (Fig. 1). The null seascape represents what one may implicitly assume if modeling evolution under varying selection with a canonical fitness landscape. The genotype fitness rank-order of the null seascape was defined as the rank order of the natural seascape at 10 μM drug concentration. The range of growth rates at low and high drug concentrations were also constrained to be the same for both seascapes. We then simulated evolution with both seascapes subject to changing drug concentration.

The simulated null seascape is shown in **Fig. 1a**. Owing to the rank-order preserving constraint, no fitness trade-offs are seen, and the most fit genotype at low drug concentration is also the most drug resistant genotype. The simulated natural seascape is shown in **Fig. 1**. Because there is no rank-preserving constraint, some genotypes exhibit fitness costs to resistance. For instance, the most drug resistant genotype, 11, exhibits the lowest growth rate at $10^{-3}\mu$M drug concentration. Rank-order fitness landscapes are shown for both simulated fitness seascapes at different drug concentrations (**Fig. 1 c-d**). Because the null seascape has a rank-preserving constraint, the rank-order fitness landscape does not change as a function of drug concentration, whereas the fitness landscape for the natural seascape exhibits 3 distinct peaks as the drug concentration changes, thus admitting non-stationary clonal dynamics as the concentration changes.

The rank-order preserving assumption has implications for predicting the trajectory of evolution under changing drug concentration. When simulating evolution with the null seascape (**Fig. 1e**), the wild type (00) quickly fixes at 10^{-3} μM drug concentration and remains the dominant strain, even as the drug concentration steps up to 10^1 and 10^5 μM. In contrast, when simulating evolution with the natural seascape (**Fig. 1f**), the 01 mutant briefly fixes at 10^{-3} μM. When the drug concentration steps up to 10^1 μM, the 00 strain becomes the most fit and subsequently takes over. Finally, at 10^5 μM, the 11 double mutant exhibits the greatest degree of resistance and fixes. The striking difference in the evolutionary trajectory between **Fig. 1e** and **f** illustrate the importance and utility of fitness seascapes in modeling evolution under changing drug concentration.

Empirical fitness seascapes reveal fitness trade-offs

Next, we explored fitness trade-offs in nature and generated fitness seascape data to parameterize an evolutionary model. Specifically, we sought to measure a novel fitness seascape and observe whether evolutionary trade-offs are seen. Using genetically engineered *E. coli* (see methods), we measured the cefotaxime dose-response curves for 16 genotypes representing a complete set of combinations of four different point mutations in the β-lactamase gene. The resulting fitness seascape is shown in **Fig. 2**. As hypothesized, we observed fitness trade-offs, or evolutionary costs to resistance. For instance, the triple and quadruple mutants, 1111 and 0111, are highly drug resistant relative to the other strains. However, they both incur a fitness cost at low concentrations of the drug, as shown by a lower growth rate at 10^{-3} μM compared to less resistant strains, such as

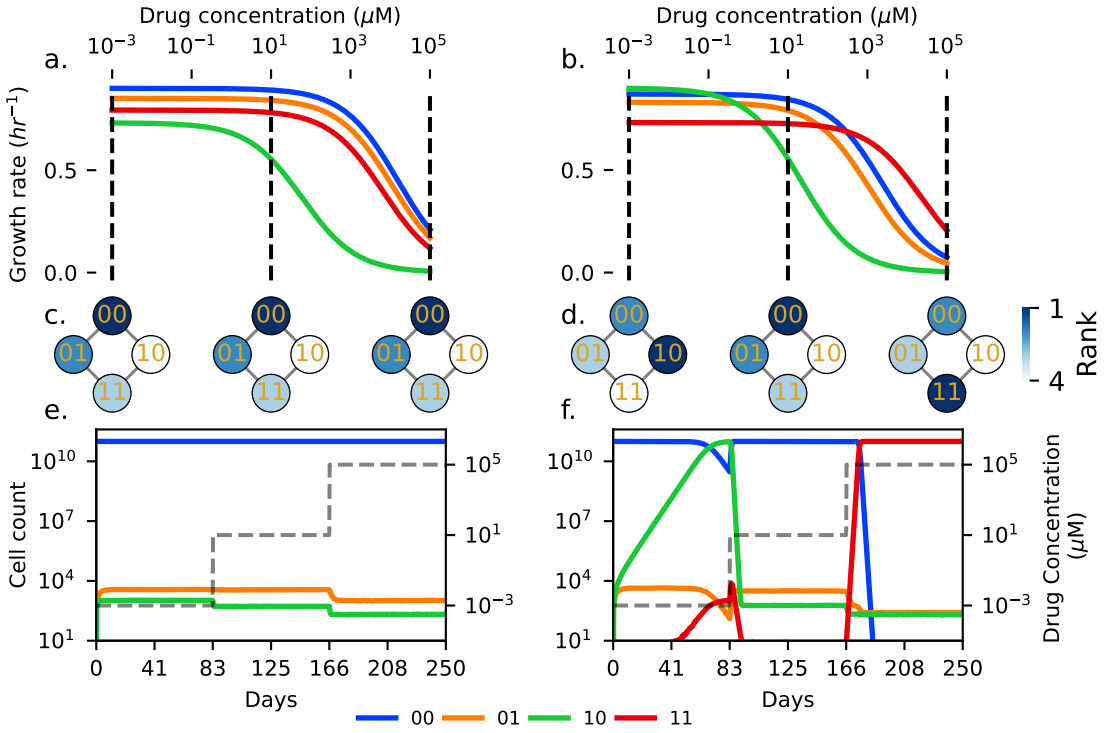

Figure 1. Evolutionary trade-offs affect evolutionary simulations under changing drug concentrations. a) Simulated fitness seascape generated with a genotype rank-preserving constraint (null seascape). Fitness landscapes are shown based on the genotype rank-order at the drug concentration given by the black vertical dotted lines. The genotype rank-order of the null seascape is the same as the rank-order of the natural seascape at drug concentration of 10 μM. **b)** Simulated fitness seascape with no rank-preserving constraint (natural seascape). Genotype rank-order and landscape topography change several times across drug concentration increases. **c-d)** Landscapes corresponding to the genotype-rank order at three different drug concentrations (10^{-3}, 10^{1}, and 10^{5} μM) for the null seascape **(c)** and natural seascape **(d)**. **e)** Evolutionary simulations with the null seascape in **(a)** subject to 3 step changes in drug concentration (average of 100 simulations). **f)** Evolutionary simulations with the natural seascape in **(b)** subject to 3 step changes in drug concentration (average of 100 simulations).

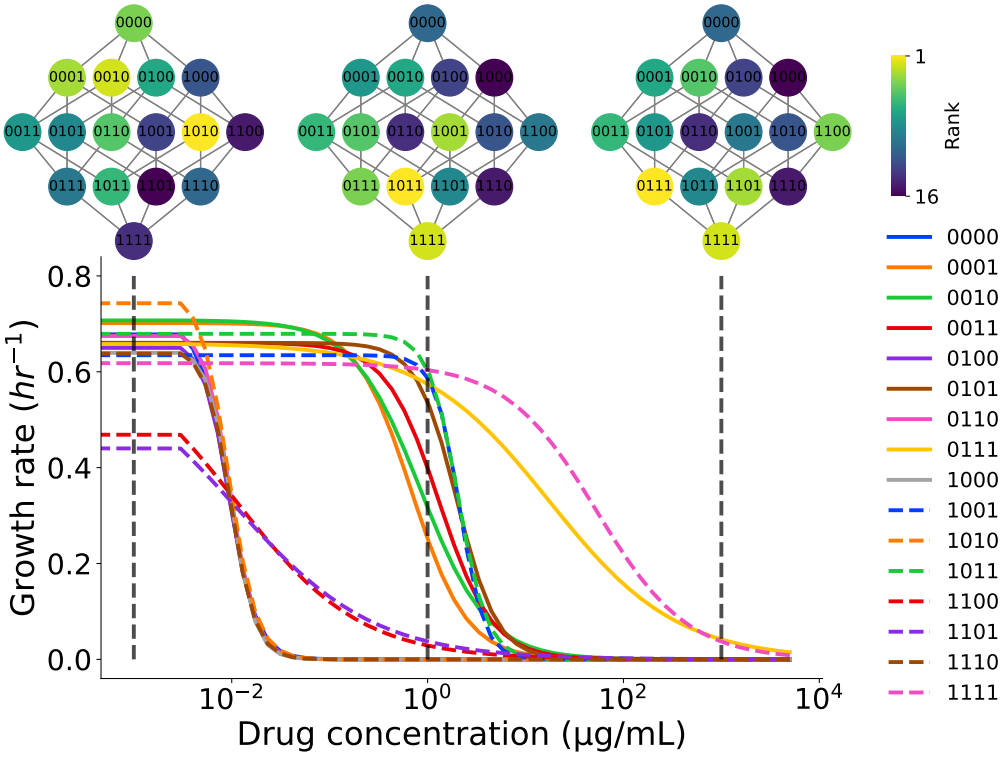

Figure 2. *E. coli* fitness seascape reveals fitness trade-offs. The fitness seascape for *E. coli* engineered with a combinatorially complete set of resistance mutations in the β-lactamase gene subject to cefotaxime. Different colors and dotted vs solid lines represent the 16 genotypes quantified. Fitness landscapes above show the rank-order fitness of genotypes at drug concentrations specified by the vertical dotted lines.

1010. Fitness landscapes, calculated as the rank-order growth rate of the 16 genotypes at three different drug concentrations, are plotted above the dose-response curves. Notably, three distinct fitness peaks are seen as the drug concentration changes: 1010 at 10^{-3} μM, 1011 at 10^{1} μM, and 0111 at 10^{5} μM. These peaks can be visualized in the corresponding inset rank-order fitness landscapes. In a patient undergoing cefotaxime therapy, the drug concentration experienced by the infectious population will traverse a broad range of fitness landscapes topographies, reaching an average C_{max} of 41 μg/mL[27], highlighting the importance of fitness seascapes in modeling the emergence of drug resistance.

Other empirical fitness seascapes in infectious disease exhibit similar evolutionary fitness trade-offs and rank-order changes. For instance, Ogbunugafor et al explored adaptive fitness landscapes in engineered *Saccharomyces cerevisia*[22] and Das et al similarly quantified an adaptive fitness landscape in *E. coli* dosed with ciprofloxacin. The presence of evolutionary trade-offs in these different microbial models and drug classes as revealed by fitness seascapes is evidence of their ubiquity in infectious disease.

Increasing rates of change in drug concentration result in lower rates of resistance

To further explore the importance and utility of fitness seascapes in modeling the emergence of drug resistance with realistic pharmacokinetic considerations, we performed two computational experiments using the empirical fitness seascape shown in **Fig. 2**. Here, we observed the effect of different rates of change in drug concentration on the probability of evolutionary escape (i.e., probability of resistance). Example data are shown in **Fig. 3**: **Fig. 3a** shows an example time trace of a population becoming resistant, while panel **Fig. 3b** shows an example time trace of a population going extinct. The corresponding drug concentration curves over time are shown in panels **Fig. 3c and d**. Both simulations have the same rate parameters (k_{abs} = 0.0004 $\mu M \cdot hr^{-1}$), but different outcomes emerged owing to the stochastic nature of the agent-based model.

As shown in **Fig. 4**, a faster rate of change in drug concentration corresponds with a lower probability of survival of the infectious agent and a lower probability of reaching a resistant genotype. A rapid rate of change, $k_{abs} = 0.0007$, resulted in 100% elimination of the infectious agent, whereas a moderate rate of change, $k_{abs} = 0.0005$ resulted in elimination of roughly 50% of the infectious agents. Furthermore, when subject to a low rate of change, $k_{abs} = 0.0004$, almost 100% of the infectious

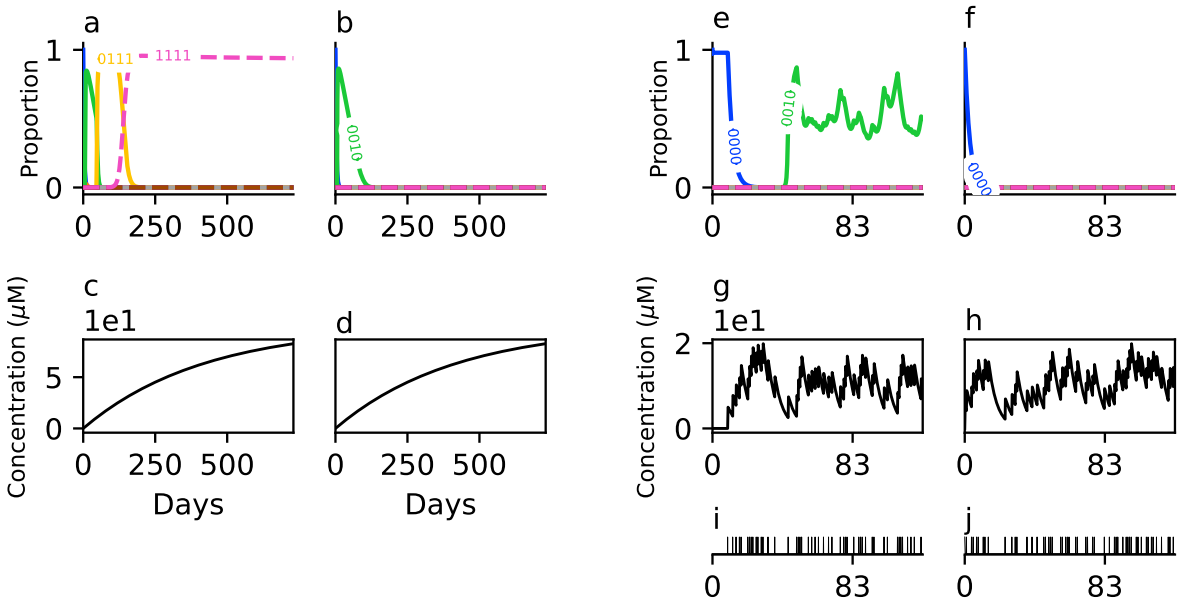

Figure 3. Representative simulations from rate of change and non-adherance experiments. All simulations leverage empirical fitness seascape data of *E. coli* dosed with cefotaxime. **a-d:** Representative data from the rate of change versus survival experiment. **a:** Example of a simulation where the population survived and became resistant. **b:** Example of a simulation where the population was eliminated. **c, d**: Corresponding drug concentration curves for both experiments. $k_{abs} = 0.0004\ \mu M \cdot hr^{-1}$ for both simulations. **e-j:** Representative data from the drug non-adherance versus survival experiment. **e:** Example of a simulation where the population survived and become resistant. **f:** Example of a simulation where the population went extinct. **g, h:** Corresponding drug concentration curves for both simulations. **i, j:** Corresponding drug regimens for both simulated patients. Vertical lines indicate days where the patient correctly took a scheduled drug dose. $p_{forget} = 0.6$ for both simulations. Evolutionary time traces are labeled with resistant genotypes.

agents survive. Similar patterns can be seen in the Kaplan-Meier curves with the primary endpoints of resistant genotype 1110 and 1111 – high rates of change result in very low rates of reaching the resistant genotypes, whereas moderate rates of change result in moderate rates of resistance and low rates of change result in 100% resistance. These results align closely with a similar *in vitro* study in *E. coli* subject to rifampicin[28].

Increasing rates of drug regimen non-adherence result in increasing rates of resistance

Patient drug regimen nonadherence is a common hindrance to effective antibiotic therapy and may contribute to drug resistance[29,30]. Indeed, nonadherence may be common even in short-term antibiotic therapy regimens[31]. To test the effects of varying levels of drug regimen nonadherence on the probability of therapy resistance with fitness seascapes, we simulated a population of patients undergoing a drug regimen to treat an infection. Simulated patients underwent a daily oral antibiotic regimen with a fixed probability of "forgetting" to take each individual dose (p_{forget}). Pharmacokinetic drug concentration curves were generated based on each simulated patients' resulting drug dosing regimen (see Eq. 2 and 3 in methods for details). Example data are shown in **Fig. 3**: **Fig. 3e** shows an example time trace of a population becoming resistant, while **Fig. 3f** shows an example time trace of a population going extinct. The corresponding drug concentration curves over time are shown in **Fig. 3g** and **Fig. 3h**. Both simulated patients had identical probabilities of forgetting to take a dose (p_{forget} = 0.6). The patients' corresponding drug dosing regimens are shown in **Fig. 3i** and **Fig. 3j**, where vertical lines represent a successfully administered drug dose.

Fig. 5 shows clear differences in the Kaplan-Meier curves of infectious agent survival and rates of resistance. In simulated patients with 100% adherence to the drug dosing regimen, $p_{forget} = 0.0$, almost 0% of the infectious population survives by the end of the study, whereas in very non-adherent patients, $p_{forget} = 0.8$, almost 100% of the infectious populations survive. Once again, similar patterns are seen in the resistance Kaplan-Meier curves. Note that the genotypes used for the endpoint here are different from those in the previous experiment – this is because the timescales of the experiments are very different, and infectious populations in the non-adherence experiment never had enough time to mutate to the triple or quadruple mutants. However, the mutants quantified here, 0010 and 0110, exhibited enough resistance to persist in some non-adherent patients.

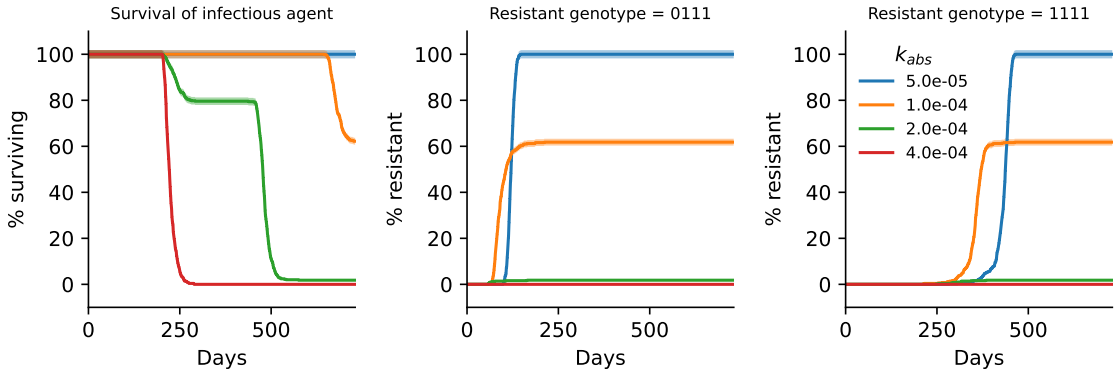

Figure 4. Differing rates of change in drug concentration result in different rates of survival and resistance of the infectious agent. Left: Kaplan-Meier curves of survival of the infectious agent under different rates of change in drug concentration (k_{abs}). **Middle:** Kaplan-Meier curves with the endpoint defined as reaching the resistant genotype 1110 under different k_{abs}. **Right**: Kaplan-Meier curves with the endpoint defined as reaching the resistant genotype 1111 under different k_{abs}. k_{abs} given in units of $\mu M \cdot hr^{-1}$. Survival is defined as at least 1 surviving infectious agent remaining within a patient. Resistance is defined as the population of the resistant genotype being at least 10% of the carrying capacity. Error bands around Kaplan-Meier curves are the standard deviation of the estimator. $N = 500$ per k_{abs}.

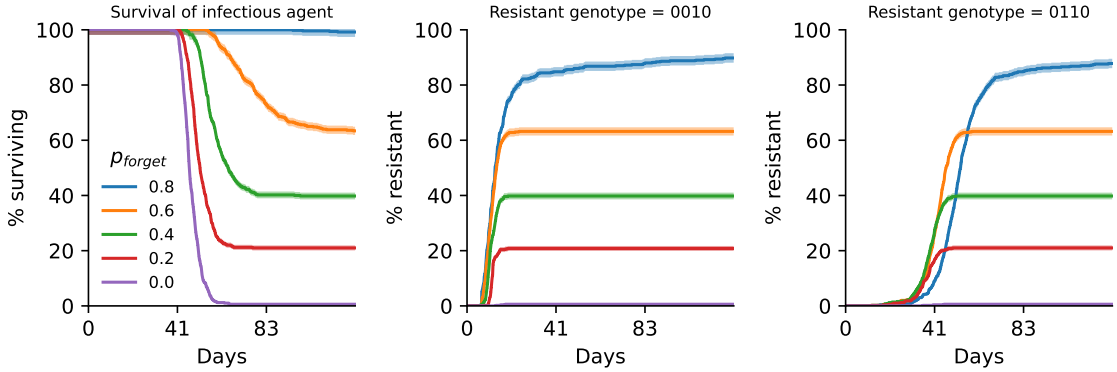

Figure 5. Increasing rates of drug regiment non-adherance result in increasing rates of survival and resistance of the infectious agent. Drug regimens were one dose of cefotaxime every 24 hours if perfectly adherent. **Left:** Kaplan-Meier curves for survival of the infectious agent for varying p_{forget}. **Middle:** Kaplan-Meier curves with the endpoint defined as reaching the resistant genotype 0010. **Right:** Kaplan-Meier curves with the endpoint defined as reaching the resistant genotype 0110. Survival is defined as at least 1 surviving infectious agent remaining within a patient. Resistance is defined as the population of the resistant genotype being at least 10% of the carrying capacity. Error bands around Kaplan-Meier curves are the standard deviation of the estimator. $N = 500$ per p_{forget}.

Survival and resistance of the infectious agent represents an ongoing, drug resistant infection in a simulated patient.

Discussion

Predicting the evolution of drug resistance is an important step in designing adaptive therapies. In this work, we have demonstrated the importance and utility of fitness seascapes in predicting evolution across a wide range of drug concentrations. In extension to the commonly studied fitness landscape model, fitness seascapes model the fitness of different genotypes subject to arbitrary drug concentrations, allowing us to predict evolution with realistic pharmacological considerations.

To study the importance of drug concentration-based tradeoffs, we first used our model to compare a simulated null seascape, with no changes in genotype rank-order, to a simulated natural seascape with no such rank-order constraint. Compared to the natural seascape, the null seascape does not model such fitness trade-offs – this scenario represents what may be implicitly employed when simulating evolution in a changing environment with a fitness landscape. In addition, since IC50 and MIC may be linearly correlated[15], the null seascape also represents the evolutionary model that may be implicitly employed when simulating evolution with a fitness landscape constructed from MIC measurements.

We next measured a fitness seascape in engineered *E. coli* subject to cefotaxime, finding evidence for fitness costs to resistance, or rank-order changes in genotype fitness as the drug concentration changes. Using this fitness seascape, we performed two computational experiments. In the first experiment, we observed the rate of evolutionary escape – or the rate of resistance – versus different rates of environmental change. Simulations with a slower rate of change (lower k_{abs}) were more likely to survive and become resistant, while those with faster rates of change (higher k_{abs}) were more likely to go extinct. This effect is likely due to the difference in mutational load; with a lower rate of change in drug concentration, the infectious population is able to proliferate more rapidly and accumulate more mutations in the population. The increased population size and proliferation rate allowed by lower rates of change in drug concentration combine to rapidly increase the mutation supply in the population. The results observed in this computational experiment are consistent with *in vitro* results reported by Lindsey et al[28]. In their experiments with *E. coli* dosed with rifampicin, they found evolutionary rescue from extinction depends on a lower rate of environmental change – few populations became resistant when subjected to a high rate of change in drug concentration.

In the second experiment, using realistic pharmacological parameters for cefotaxime, we simulated patients undergoing a drug regimen for an infection with different rates of non-adherence. A higher rate of non-adherance was found to be associated with a higher rate of survival of the infectious agent and a higher rate of resistance. This non-adherance experiment with simulated patients highlights the power of fitness seascapes – as reflected in **Fig. 3**, the serum drug concentration curve for each simulated patient is unique, and the concentration varies over several orders of magnitude. Each new drug concentration represents a distinct landscape where different evolutionary dynamics occur.

There are many potential applications of the modeling framework presented here. For example, much interest has been given to optimizing antibiotic cycling to avoid resistance in bacteria, in both computational studies with fitness landscapes[10,32–35], *in vitro* studies[36], and clinical trials[37]. In these models, different antibiotics are associated with different fitness landscapes. By leveraging fitness seascapes, we can greatly increase the number of possible distinct fitness landscape topographies accessible with a given set of antibiotics. Each individual drug may produce several different changes in genotype fitness rank as a function of antibiotic concentration. Furthermore, one could modulate the antibiotic dose to control evolution and avoid resistance with fitness seascapes[38]. Along with antibiotic cycling, optimizing drug dosing regimens is another natural application of our work. By varying the timing and dose of an antibiotic therapy, we may discover parameter ranges that reliably avoid resistance *in silico*. Then, using empirical knowledge of patient preferences[31,39], we may deliver dosing regimens that are both amenable to patient adherence and successful elimination of the infection.

In addition to time-varying drug concentrations due to pharmacokinetic effects, tissue drug absorption results in selection gradients in patients undergoing therapy. Indeed, using a computational model, Moreno-Gamez et al[40] showed that variable rates of drug distribution within the body may favor the evolution of resistance, and Feder et al[41] use a similar model to explain triple drug resistance in HIV. Fitness seascapes will likely prove useful in modeling these dynamics as well when integrated into spatial models of evolution, as the selection pressures of variable drug concentrations are immediately reflected in the fitness seascape model.

A similar platform of modeling evolution with fitness seascapes was introduced by Engelstädter[42]. Here, we have expanded on their work along several domains. First, we have developed an agent-based model of evolution on fitness seascapes, FEArS, that allows for arbitrary empirical and simulated fitness seascapes, arbitrary drug concentrations, an arbitrary number of genotypes, and a wide array of experiments and experimental parameters. Notably, FEArS models cell death, allowing the for the study of extinction versus resistance experiments, and is agent-based, allowing for the study of stochastic emergence of resistance. Furthermore, we have employed empirical fitness seascapes in our computational studies and qualitatively compared the results to *in vitro* studies. Finally, we have demonstrated the utility of fitness seascapes using an experiment with simulated patients undergoing a drug regimen nonadherence study, finding that greater rates of nonadherence result in greater rates of resistance.

There are several limitations to this work. First, the 4-allele fitness seascape quantified here represents only a small set of the possible resistance mutations. For instance, off-target mutations in genes regulating drug efflux pumps or cell metabolism may also contribute to resistance. A more robust method for generating genotype-fitness mappings in an unbiased way will likely be necessary for generalizing these results. Furthermore, the evolutionary model employed here only represents well-mixed *E. coli* growing in a petri dish– we do not model immune system interactions, spatial considerations, or frequency-dependent fitness effects. A more complete evolutionary model will be important for future clinical applications of this work.

Our work represents the first application of fitness seascapes to predicting the emergence of resistance in evolutionary medicine. Our results suggest that explicit modeling of evolutionary trade-offs is important for predicting evolution under time-varying drug concentration. Future applications of this modeling framework may be useful for optimizing drug dosing regimens *in silico* and designing adaptive therapies.

Methods

Estimating dose-response curves

We measured a combinatorially complete seascape to cefotaxime using genetically engineered DH5-α *E. coli* provided to us by the Weinreich Lab at Brown University[9]. These strains have combinations of four point mutations in the β-lactamase gene. Each point mutation increases resistance to β-lactam antibiotics. To measure the seascapes, strains are inoculated into MH+ampicillin and allowed to grow up overnight in a bacterial shaking incubator set to 37°C and 225rpm. Once grown up, a 1:500 dilution of bacteria into fresh media is performed, and the bacteria are plated against cefotaxime following a 10-fold microdilution scheme. The plate is incubated for 12 hours in a Tecan Microplate Reader at 37°C and 225rpm, and OD600 scans of the entire plate are taken every 20 minutes. OD600 data were normalized to the maximum measured OD value and normalized data were fit to a Hill function to obtain IC50 values which are used to parameterize genotype-specific dose-response curves. Raw data are available in the github repository (https://github.com/eshanking/seascapes_figures).

Computational model

We developed an agent-based algorithm, FEArS (Fast Evolution on Arbitrary Seascapes), to simulate evolution on fitness seascapes (**Fig. 6**). FEArS models carrying capacity, agent replication, mutation, death, and arbitrary drug dosing regimens. With this algorithm, genotypes are modeled as a bit string of n alleles, with 0 representing the wild type and 1 representing a point mutation at that location, yielding 2^n possible combinations. For example, in a 4-allele scenario, 0000 represents the wild type and 1111 represents the quadruple mutant. Agents mutate from one genotype to another by changing a single bit from 1 to 0 or vice-versa. In simulations, the drug concentration is updated at every time step (1 hour unless otherwise specified) according to the drug dosing regimen and the fitness of each genotype is updated according to the fitness seascape.

Patient drug serum concentrations, $c(t)$, are modeled with a 1-compartment pharmacokinetic model,

$$c(t) = c_{max}[e^{-k_{elim}t} - e^{-k_{abs}t}], \tag{1}$$

where k_{abs} and k_{elim} represent absorption and elimination rates and c_{max} represents the maximum drug concentration. Drug doses are simulated with an impulse train, with each impulse representing a dose (**Fig. 3I and J**). Serum concentration over time for each patient is computed by convolving the drug dose impulse train with the pharmacokinetic model (**Fig. 3G and H**). Formally, this is done by generating a set (K) of numbers representing the time of each scheduled drug dose. Then, for each patient, a random subset of drug doses are removed from K, with each drug dose having a constant probability of being removed (p_{forget}), resulting in the set of drug doses that the simulated patient correctly self administered (K_a). A Dirac comb (Eq. 2) is generated using K_a with the period equal to the time between drug doses, and the resulting impulse train is convolved with the pharmacokinetic model in Eq. 1 to generate the simulated patient's serum drug concentration (Eq. 3).

$$III_a(t) = \sum_{k \in K_a} \delta(t - kT) \tag{2}$$

$$c_{patient}(t) = c(t) \circledast III_a(t) \tag{3}$$

Computational parameters

Death[43] and mutation[44] rates were inferred from existing literature on *in vitro E. coli* models. As these *in vitro* systems do not include immune system interactions, we expect the death rate to be much higher in the clinical setting. As such, these computational experiments represent dosing an *in vitro E. coli* culture. Cefotaxime pharmacokinetic parameters were estimated from a clinical population study[27].

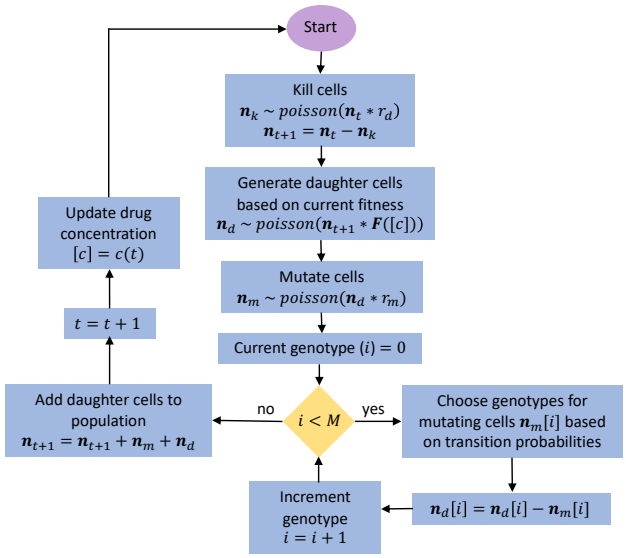

Figure 6. FEArS algorithm flow chart. n_t is a vector of genotype populations at time t, τ_d is the death rate, $F([c])$ is a vector of genotype fitness at drug concentration c, r_m is the mutation rate, and M is total number of genotypes. Cell death, division, and mutation number are modeled with the Poisson distribution. The specific mutation for each cell is chosen by picking from a uniform distribution of all possible genetic changes in the set of alleles under study. Code can be found at https://github.com/eshanking/seascapes_figures.

Computational Parameters		
Parameter	Value	Citation
Death rate	$0.0144hr^{-1}$	Gonidakis et al[43]
Mutation rate	$1.4x10^{-8}$ per bp	Jee et al[44]
Cefotaxime absorption rate	$0.95hr^{-1}$	Patel et al[27]
Cefotaxime elimination rate	$0.00839hr^{-1}$	Patel et al[27]

References

1. Stearns, S. C. Evolutionary medicine: Its scope, interest and potential. *Proc. Royal Soc. B: Biol. Sci.* **279**, 4305–4321, DOI: 10.1098/rspb.2012.1326 (2012).
2. Grunspan, D. Z., Nesse, R. M., Barnes, M. E. & Brownell, S. E. Core principles of evolutionary medicine. *Evol. Medicine, Public Heal.* **2018**, 13–23, DOI: 10.1093/emph/eox025 (2018).
3. Perry, G. H. Evolutionary medicine. *eLife* **10**, e69398, DOI: 10.7554/eLife.69398 (2021).
4. Chmielecki, J. *et al.* Optimization of dosing for egfr-mutant non–small cell lung cancer with evolutionary cancer modeling. *Sci. Transl. Medicine* **3**, DOI: 10.1126/scitranslmed.3002356 (2011).
5. Chakrabarti, S. & Michor, F. Pharmacokinetics and drug interactions determine optimum combination strategies in computational models of cancer evolution. *Cancer Res.* **77**, 3908–3921, DOI: 10.1158/0008-5472.CAN-16-2871 (2017).
6. Poels, K. E. *et al.* Identification of optimal dosing schedules of dacomitinib and osimertinib for a phase i/ii trial in advanced egfr-mutant non-small cell lung cancer. *Nat. Commun.* **12**, 3697, DOI: 10.1038/s41467-021-23912-4 (2021).
7. Maltas, J. & Wood, K. B. Pervasive and diverse collateral sensitivity profiles inform optimal strategies to limit antibiotic resistance. *PLoS biology* **17**, e3000515 (2019).
8. Iram, S. *et al.* Controlling the speed and trajectory of evolution with counterdiabatic driving. *Nat. Phys.* **17**, 135–142 (2021).

9. Weinreich, D. M., Delaney, N. F., DePristo, M. A. & Hartl, D. L. Darwinian Evolution Can Follow Only Very Few Mutational Paths to Fitter Proteins. *Science* **312**, 111–114, DOI: 10.1126/science.1123539 (2006).

10. Goulart, C. P. *et al.* Designing antibiotic cycling strategies by determining and understanding local adaptive landscapes. *PLoS ONE* **8**, e56040, DOI: 10.1371/journal.pone.0056040 (2013).

11. Fragata, I., Blanckaert, A., Dias Louro, M. A., Liberles, D. A. & Bank, C. Evolution in the light of fitness landscape theory. *Trends Ecol. & Evol.* **34**, 69–82, DOI: 10.1016/j.tree.2018.10.009 (2019).

12. Kouyos, R. D. *et al.* Exploring the Complexity of the HIV-1 Fitness Landscape. *PLoS Genet.* **8**, e1002551, DOI: 10.1371/journal.pgen.1002551 (2012).

13. Maltas, J., McNally, D. M. & Wood, K. B. Evolution in alternating environments with tunable interlandscape correlations. *Evolution* **75**, 10–24, DOI: 10.1111/evo.14121 (2021).

14. Gillespie, J. H. Some properties of finite populations experiencing strong selection and weak mutation. *The Am. Nat.* **121**, 691–708 (1983).

15. Brown, K. M. *et al.* Compensatory mutations restore fitness during the evolution of dihydrofolate reductase. *Mol. Biol. Evol.* **27**, 2682–2690, DOI: 10.1093/molbev/msq160 (2010).

16. Lagator, M., Colegrave, N. & Neve, P. Selection history and epistatic interactions impact dynamics of adaptation to novel environmental stresses. *Proc. Royal Soc. B: Biol. Sci.* **281**, 20141679, DOI: 10.1098/rspb.2014.1679 (2014).

17. Costanzo, M. S., Brown, K. M. & Hartl, D. L. Fitness trade-offs in the evolution of Dihydrofolate reductase and drug resistance in plasmodium falciparum. *PLoS One* **6**, DOI: 10.1371/journal.pone.0019636 (2011).

18. Maisnier-Patin, S. & Andersson, D. I. Adaptation to the deleterious effects of antimicrobial drug resistance mutations by compensatory evolution. *Res. Microbiol.* **155**, 360–369, DOI: 10.1016/j.resmic.2004.01.019 (2004).

19. Farrokhian, N. *et al.* Measuring competitive exclusion in non-small cell lung cancer. *bioRxiv* DOI: 10.1101/2020.09.18.303966 (2020).

20. Lässig, M., Mustonen, V. & Walczak, A. M. Predicting evolution. *Nat. Ecol. Evol.* **1**, 0077 (2017).

21. Merrell, D. J. *The Adaptive Seascape: The Mechanism of Evolution* (University of Minnesota Press, 1994), minne ed. edition edn.

22. Ogbunugafor, C. B., Wylie, C. S., Diakite, I., Weinreich, D. M. & Hartl, D. L. Adaptive Landscape by Environment Interactions Dictate Evolutionary Dynamics in Models of Drug Resistance. *PLoS Comput. Biol.* **12**, 1–20, DOI: 10.1371/journal.pcbi.1004710 (2016).

23. Das, S. G., Direito, S. O., Waclaw, B., Allen, R. J. & Krug, J. Predictable properties of fitness landscapes induced by adaptational tradeoffs. *eLife* **9**, e55155, DOI: 10.7554/eLife.55155 (2020).

24. Mustonen, V. & Lässig, M. From fitness landscapes to seascapes: non-equilibrium dynamics of selection and adaptation. *Trends Genet.* **25**, 111–119, DOI: 10.1016/j.tig.2009.01.002 (2009).

25. Agarwala, A. & Fisher, D. S. Adaptive walks on high-dimensional fitness landscapes and seascapes with distance-dependent statistics. *Theor. Popul. Biol.* **130**, 13–49, DOI: 10.1016/j.tpb.2019.09.011 (2019).

26. Rosenbloom, D. I. S., Hill, A. L., Rabi, S. A., Siliciano, R. F. & Nowak, M. A. Antiretroviral dynamics determines hiv evolution and predicts therapy outcome. *Nat. Medicine* **18**, 1378–1385, DOI: 10.1038/nm.2892 (2012).

27. Patel, K. B., Nicolau, D. P., Nightingale, C. H. & Quintiliani, R. Pharmacokinetics of cefotaxime in healthy volunteers and patients. *Diagn. Microbiol. Infect. Dis.* **22**, 49–55, DOI: 10.1016/0732-8893(95)00072-I (1995).

28. Lindsey, H. A., Gallie, J., Taylor, S. & Kerr, B. Evolutionary rescue from extinction is contingent on a lower rate of environmental change. *Nature* **494**, 463–467, DOI: 10.1038/nature11879 (2013).

29. Sorensen, S. V. *et al.* Cost and clinical consequence of antibiotic non-adherence in acute exacerbations of chronic bronchitis. *The Int. J. Tuberc. Lung Dis. The Off. J. Int. Union Against Tuberc. Lung Dis.* **13**, 945–954 (2009).

30. Pechère, J.-C., Hughes, D., Kardas, P. & Cornaglia, G. Non-compliance with antibiotic therapy for acute community infections: a global survey. *Int. J. Antimicrob. Agents* **29**, 245–253, DOI: 10.1016/j.ijantimicag.2006.09.026 (2007).

31. Kardas, P. Patient compliance with antibiotic treatment for respiratory tract infections. *J. Antimicrob. Chemother.* **49**, 897–903, DOI: 10.1093/jac/dkf046 (2002).

32. Kouyos, R. D., Abel zur Wiesch, P. & Bonhoeffer, S. Informed switching strongly decreases the prevalence of antibiotic resistance in hospital wards. *PLoS Comput. Biol.* **7**, e1001094, DOI: 10.1371/journal.pcbi.1001094 (2011).

33. Mira, P. M. *et al.* Rational design of antibiotic treatment plans: A treatment strategy for managing evolution and reversing resistance. *PLOS ONE* **10**, e0122283, DOI: 10.1371/journal.pone.0122283 (2015).

34. Nichol, D. *et al.* Steering evolution with sequential therapy to prevent the emergence of bacterial antibiotic resistance. *PLOS Comput. Biol.* **11**, e1004493, DOI: 10.1371/journal.pcbi.1004493 (2015).

35. Nichol, D. *et al.* Antibiotic collateral sensitivity is contingent on the repeatability of evolution. *Nat. Commun.* **10**, 334, DOI: 10.1038/s41467-018-08098-6 (2019).

36. Kim, S., Lieberman, T. D. & Kishony, R. Alternating antibiotic treatments constrain evolutionary paths to multidrug resistance. *Proc. Natl. Acad. Sci.* **111**, 14494–14499, DOI: 10.1073/pnas.1409800111 (2014).

37. Abel zur Wiesch, P., Kouyos, R., Abel, S., Viechtbauer, W. & Bonhoeffer, S. Cycling empirical antibiotic therapy in hospitals: Meta-analysis and models. *PLoS Pathog.* **10**, e1004225, DOI: 10.1371/journal.ppat.1004225 (2014).

38. Iram, S. *et al.* Controlling the speed and trajectory of evolution with counterdiabatic driving. *Nat. Phys.* **17**, 135–142, DOI: 10.1038/s41567-020-0989-3 (2021).

39. Claxton, A. J., Cramer, J. & Pierce, C. A systematic review of the associations between dose regimens and medication compliance. *Clin. Ther.* **23**, 1296–1310, DOI: 10.1016/S0149-2918(01)80109-0 (2001).

40. Moreno-Gamez, S. *et al.* Imperfect drug penetration leads to spatial monotherapy and rapid evolution of multidrug resistance. *Proc. Natl. Acad. Sci.* **112**, E2874–E2883, DOI: 10.1073/pnas.1424184112 (2015).

41. Feder, A. F., Harper, K. N., Brumme, C. J. & Pennings, P. S. Understanding patterns of hiv multi-drug resistance through models of temporal and spatial drug heterogeneity. *eLife* **10**, e69032, DOI: 10.7554/eLife.69032 (2021).

42. Engelstädter, J. Fitness landscapes emerging from pharmacodynamic functions in the evolution of multidrug resistance. *J. Evol. Biol.* **27**, 840–853, DOI: 10.1111/jeb.12355 (2014).

43. Gonidakis, S. & Longo, V. D. Assessing chronological aging in bacteria. *Methods Mol. Biol.* **965**, 421–437, DOI: 10.1007/978-1-62703-239-1_28 (2013).

44. Jee, J. *et al.* Rates and mechanisms of bacterial mutagenesis from maximum-depth sequencing. *Nature* **534**, 693–696, DOI: 10.1038/nature18313 (2016).

Acknowledgements

We acknowledge the Weinreich Lab at Brown University for providing the genetically engineered *E. coli* strains used in this work. This work was made possible by NIH grants 5R37CA244613-03, 5T32GM007250-46, and